Single-Pass
Ion Cyclotron Resonance Absorption

Boris N. Breizman and Alexey V. Arefiev
Institute for Fusion Studies, The University of Texas, Austin, Texas 78712

(Dated: July 17, 2000)

Abstract

The ion response to the rf-field during single-pass ion-cyclotron resonance heating (ICRH) can be essentially nonlinear. This paper presents a self-consistent theory of the rf-wave propagation and ion motion through the resonance. An important ingredient of the problem is the ion flow along the magnetic field. The flow velocity limits the time the ions spend at the resonance, which in turn limits the ion energy gain. A feature that makes the problem nonlinear is that the flow accelerates under the effect of the ∇B force and rf-pressure. This acceleration can produce a steep decrease in the plasma density at the resonance, resulting in partial reflection of the incident wave.

I. INTRODUCTION

This work has been motivated by the Variable Specific Impulse Magnetoplasma Rocket (VASIMR) project [1, 2], one of the prospective plasma-based space propulsion systems [3]. The VASIMR concept employs ion-cyclotron-resonance-heating (ICRH) as the mechanism for rf-power deposition in the plasma. The device has a magnetic mirror configuration and consists of three main components: the low energy plasma source, ICRH section, and magnetic nozzle. The source creates a cold plasma that flows along the field lines, down the magnetic field gradient, towards the ICRH section. In the ICRH section, the decreasing ion gyro-frequency ω_{ci} matches the rf-antenna frequency ω to ensure wave energy conversion into the ion gyro-motion. The heated plasma then passes through the magnetic nozzle that (a) transforms the ion gyro-rotation into a fast motion along the field lines and (b) forms a highly directed superalfvenic outgoing flow to maximize the thrust.

The ICRH in VASIMR has two distinct features. First, each ion passes the resonance only once, gaining an energy that is much greater than the initial energy. Second, the ion motion is collisionless, i.e. the energy gain is limited not by collisions but by the time the ion spends at the resonance while moving along the field lines. Therefore, the ion final energy, as well as the rf-power absorption efficiency, should depend on the incident-flow velocity. If the flow is sufficiently fast, its velocity will not change significantly at the resonance. As a result, the ion density will also be nearly constant throughout the resonance. In this regime, ion flux through the resonance turns out to be sufficient to absorb all the rf-power. Technically, the description of the fast flow case is a linear problem. In contrast with the fast incoming flow, the slow flow case is essentially nonlinear. Slow ions can be significantly accelerated along the magnetic field even before they reach their full rotational energy. The driving forces responsible for their acceleration are the ∇B force and rf-pressure. Depending on plasma parameters and incident rf-power, the acceleration distance can either extend over many wavelengths or be as short as a fraction of wavelength. In both limits, the nonlinear problem allows approximate analytical solutions. In the limit of long acceleration distance, our solution involves WKB approximation. In the opposite limit, we exploit the narrowness

of the resonance.

The paper is organized in the following way. In Sec.II, we introduce a basic set of nonlinear fluid-type equations for the electromagnetic field of a circular polarized wave and the steady-state ion flow through the resonance. In Sec.III, we present a linear theory of wave energy conversion into ion rotational energy. This section is very closely related to the well-known linear magnetic beach problem [4] that exhibits 100% conversion efficiency. An interesting new element of Sec.III is the WKB-type conversion mechanism. The corresponding solution indicates that this type of conversion can be described as a propagation of a properly chosen WKB mode in an inhomogeneous medium without any mode coupling effects. In Sec.IV, we analyze the nonlinear regimes of ion-cyclotron absorption. We find that the absorption efficiency is still 100%, as long as the WKB approximation is applicable. We also describe the nonlinear absorption in the anti-WKB (narrow resonance) limit, in which case we predict a steep density drop at the resonance and substantial reflection of the rf-power. In Sec.V, we present a numerical model that reproduces our analytical results and allows us to quantitatively extend the description to a broader range of parameters. In particular, this model quantifies the effect of nonlinear reflection. Finally, in Sec.VI, we summarize the results.

II. BASIC EQUATIONS NEAR THE RESONANCE

We consider collisionless plasma with cold ions in an equilibrium axisymmetric mirror magnetic field $\mathbf{B}_0 = (B_{0r}; 0; B_{0z})$, where z is the axis of symmetry. We assume that B_{0z} is positive, with $B_{0z} \gg B_{0r}$, and that B_{0z} decreases monotonically along z.

We consider a wave that is launched nearly parallel to the magnetic field lines, so that one can neglect the dependence of the wave fields on the perpendicular coordinates. We choose $z = 0$ to be the location of the ion-cyclotron resonance, and we use the following approximation for the ion gyro-frequency $\omega_{ci} = eB_0/m_i c$ near the resonance

$$\omega_{ci} = \omega(1 - z/L). \tag{II.1}$$

Here, ω is the wave frequency and L is the characteristic scale-length of the equilibrium

magnetic field.

The electric and magnetic fields of the wave are determined by Maxwell's equations:

$$curl\mathbf{E} = -\frac{1}{c}\frac{\partial \mathbf{B}}{\partial t}, \tag{II.2}$$

$$curl\mathbf{B} = \frac{4\pi}{c}\mathbf{j}, \tag{II.3}$$

where $\mathbf{j}$ is the plasma current. We have neglected the displacement current in Eq.(II.3), which is justified when

$$\omega_{pi} \gg \omega_{ci}, \tag{II.4}$$

where $\omega_{pi} = \sqrt{4\pi ne^2/m_i}$ is the ion plasma frequency. High electron conductivity eliminates E_z in our problem, which allows us to replace the z-component of Eq.(II.3) by

$$E_z = 0. \tag{II.5}$$

Since the x and y derivatives of the fields are small near the resonance, the transverse components of Maxwell's equations reduce to

$$\frac{\partial E_y}{\partial z} = \frac{1}{c}\frac{\partial B_x}{\partial t}, \qquad \frac{\partial E_x}{\partial z} = -\frac{1}{c}\frac{\partial B_y}{\partial t}, \tag{II.6}$$

$$\frac{\partial B_y}{\partial z} = -\frac{4\pi}{c}j_x, \qquad \frac{\partial B_x}{\partial z} = \frac{4\pi}{c}j_y. \tag{II.7}$$

Here, j_x and j_y are the components of the ion current given by

$$j_x = enV_x j_y = enV_y, \tag{II.8}$$

where n is the ion density and V_x and V_y are the ion velocity components. The electron current is not included in Eq.(II.7), since its transverse components are much smaller than the ion current near the resonance.

In order to find V_x and V_y, we use the corresponding components of the ion momentum balance equation together with Eq.(II.1) for ω_{ci}:

$$\frac{\partial V_x}{\partial t} + V_z\frac{\partial V_x}{\partial z} = \frac{eE_x}{m_i} + \omega(1 - z/L)V_y, \tag{II.9}$$

$$\frac{\partial V_y}{\partial t} + V_z \frac{\partial V_y}{\partial z} = \frac{eE_y}{m_i} - \omega(1 - z/L)V_x, \tag{II.10}$$

where V_z is the parallel component of the ion velocity.

We assume a steady-state ion flow through the resonance, so that

$$nV_z = const. \tag{II.11}$$

The quantities n and V_z are time-independent, whereas the transverse components of all vectors oscillate at the wave frequency.

The spatial dependence of V_z is determined by the longitudinal momentum balance equation

$$m_i V_z \frac{\partial V_z}{\partial z} = -\mu \frac{\partial B_{0z}}{\partial z} + \frac{e}{c} \langle V_x B_y - V_y B_x \rangle - m_i \frac{c_s^2}{n} \frac{\partial n}{\partial z}. \tag{II.12}$$

with a convective term on the left-hand side and three longitudinal forces on the right-hand side. The angular brackets in this equation, as well as in the subsequent equations, stand for time averaging over the wave period. The three forces in Eq.(II.12) are:

- The ∇B_0-force

$$-\mu \frac{\partial B_{0z}}{\partial z},$$

which is associated with the ion magnetic moment $\mu = m_i \left\langle V_x^2 + V_y^2 \right\rangle / 2B_{0z}$.

- The time averaged Lorentz force from the wave

$$\frac{e}{c} \langle (\mathbf{V} \times \mathbf{B})_z \rangle = \frac{e}{c} \langle V_x B_y - V_y B_x \rangle .$$

- The force associated with the ambipolar electric field:

$$-m_i \frac{c_s^2}{n} \frac{\partial n}{\partial z},$$

were $c_s = \sqrt{T_e/m_i}$ is the ion acoustic velocity and T_e is the electron temperature.

The time averaging procedure in Eq.(II.12) requires that the ions complete many cycles over their gyro-orbit while they move through the resonance, i.e.

$$\tau_r \omega_{ci} \gg 1, \tag{II.13}$$

where τ_r is the time ion spends in the resonance area.

We limit our consideration to a circular polarized wave that rotates in the "ion" direction. The electric field of this wave has the form:

$$E_x = \frac{1}{2}\left[E_+(z)\mathrm{e}^{-i\omega t} + c.c.\right], \tag{II.14}$$

$$E_y = \frac{1}{2}\left[E_+(z)\mathrm{e}^{-i\omega t - i\pi/2} + c.c.\right], \tag{II.15}$$

where $E_+(z)$ is a complex amplitude. The magnetic field and the ion velocity components also have the form of Eqs.(II.14) and (II.15) with B_+ and V_+ the corresponding amplitudes.

The polarization constraints, (II.14) and (II.15), allow us to reduce Eqs.(II.6)-(II.12) to a closed set of equations for E_+, B_+, V_+, V_z, and n. The equations read

$$\frac{\partial E_+}{\partial z} = \frac{\omega}{c}B_+, \tag{II.16}$$

$$\frac{\partial B_+}{\partial z} = -\frac{4\pi i}{c}neV_+, \tag{II.17}$$

$$V_z\frac{\partial V_+}{\partial z} = \frac{e}{m_i}E_+ + i\omega\frac{z}{L}V_+, \tag{II.18}$$

$$j \equiv nV_z = const, \tag{II.19}$$

$$V_z\frac{\partial V_z}{\partial z} = \frac{|V_+|^2}{2L} - \frac{1}{8\pi m_i n}\frac{\partial |B_+|^2}{\partial z} - \frac{c_s^2}{n}\frac{\partial n}{\partial z}. \tag{II.20}$$

The boundary conditions for this set of equations are

$$V_+(-\infty) = 0 \tag{II.21}$$

(absence of the ion gyro motion at $z = -\infty$) and

$$E_+(+\infty) = 0, B_+(+\infty) = 0 \tag{II.22}$$

(evanescent wave fields downstream).

In addition we must specify the power flux in the incident wave, the incident ion flux, and the ion flow velocity at $z \to -\infty$. It should be noted that the ion flow must be supersonic to justify this formulation of the problem.

The key quantities to be determined from Eqs.(II.16)-(II.20) are the ion energy gain and the reflection coefficient for the wave.

We start our analysis of Eqs.(II.16)-(II.20) from the limiting case of fast incoming flow, which means that V_z and n can be treated as constants in the resonance area. This simplification "linearizes" the problem. The linear analysis (Sec.III) will then be followed by the analysis of slow flow regime (Sec.IV) that is essentially nonlinear.

III. LINEAR THEORY

The fast flow assumption of nearly constant V_z decouples Eqs.(II.16)-(II.18) from Eqs.(II.19) and (II.20). We can thus combine Eqs.(II.16)-(II.18) into a single linear equation for E_+:

$$i\gamma \frac{\partial^3 E_+}{\partial s^3} + s\frac{\partial^2 E_+}{\partial s^2} - E_+ = 0, \tag{III.1}$$

where

$$s \equiv \frac{L\omega_{pi}^2}{c^2} z, \gamma \equiv \frac{V_z}{L\omega}\left(\frac{L\omega_{pi}}{c}\right)^4 > 0. \tag{III.2}$$

It should be noted that this equation differs from the "Standard Equation" discussed in [5]. Unlike the "Standard Equation" which only contains the even derivatives of the field, Eq.(III.1) contains an odd derivative $\partial^3 E_+/\partial s^3$. This difference in symmetry is due to the directed ion flow along the field lines. The flow is more important in our problem than the ion thermal motion since we assume that the flow is supersonic.

All independent solutions of Eq.(III.1) can be written in the form of a contour integral in the complex k-plane

$$E_+(s) = \int_C E(k) e^{iks} dk, \tag{III.3}$$

where $E(k)$ is the Laplace-image of $E_+(s)$ and contour C has to be specified for each solution. Substitution of Eq.(III.3) into Eq.(III.1) with subsequent integration by parts gives

$$\int_C \left[\gamma k^3 E - i\frac{d}{dk}(k^2 E) - E\right] dk = 0, \tag{III.4}$$

provided that

$$k^2 E e^{iks}\Big|_a^b = 0 \tag{III.5}$$

for all real values of s. We use notations a and b for the end points of the contour C. It follows from Eq.(III.4) that

$$E(k) = \frac{E_*}{k^2} e^{-i/k - i\gamma k^2/2}, \tag{III.6}$$

where E_* is an arbitrary constant.

We now use Eqs.(II.16), (II.17), (III.3), and (III.6) to find V_+:

$$V_+ = -i\frac{e}{m_i}\left(\frac{\omega_{pi}L}{c}\right)^2 \frac{E_*}{\omega}\int_C dk e^{\varphi}, \tag{III.7}$$

where

$$\varphi \equiv iks - i/k - i\gamma k^2/2. \tag{III.8}$$

In order to satisfy Eq.(III.5), the end points of the contour C must be either at infinity (in the sectors where the products $\mathrm{Re}(a)\mathrm{Im}(a)$ and $\mathrm{Re}(b)\mathrm{Im}(b)$ are negative), or at the origin. In the latter case, the contour must approach the origin from the upper half-plane. The contours that give three independent solutions of Eq.(III.1) are shown in Fig.1.

Of the three contours shown in Fig.1, C_2 is the only one that meets the boundary conditions (II.21) and (II.22). In order to demonstrate this, we will consider the asymptotic behaviour of the solution (III.3), (III.6), and (III.7) for $C = C_2$.

In the asymptotic regime, integrals (III.3) and (III.7) can be evaluated by choosing the integration contour C_2 to go through the stationary phase points (saddle points) in which

$$\frac{d\varphi}{dk} = 0, \tag{III.9}$$

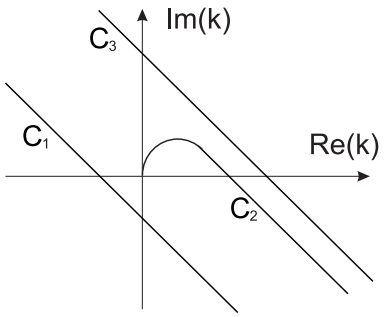

FIG. 1: Independent contours for Eq. (III.1) in the k-plane.

or, equivalently,

$$\gamma k^3 - sk^2 - 1 = 0. \tag{III.10}$$

For very large negative values of s, the only accessible saddle point for C_2 is $k_1 = 1/\sqrt{-s}$. The line of the steepest descent crosses the real axis at an angle of $-\pi/4$. The contribution to Eq.(III.3) from this point represents the incident wave propagating towards the resonance:

$$E_+ = E_* \sqrt{\pi} (-s)^{1/4} \mathrm{e}^{-2i\sqrt{-s} - i\pi/4}. \tag{III.11}$$

The corresponding expression for V_+ is

$$V_+ = -i \frac{e}{m_i} \left(\frac{\omega_{pi} L}{c} \right)^2 \frac{\sqrt{\pi}}{(-s)^{3/4}} \frac{E_*}{\omega} \mathrm{e}^{-2i\sqrt{-s} - i\pi/4}. \tag{III.12}$$

Note that $V_+ \to 0$ as $s \to -\infty$, in agreement with the boundary condition given by Eq.(II.21).

For very large positive values of s, the relevant saddle points are $k_2 = s/\gamma$ and $k_3 = i/\sqrt{s}$. The corresponding lines of the steepest descent cross the real axis at angles of $-\pi/4$ and $\pi/2$, respectively (see Fig.2). The contribution from k_2 represents the ion gyro-velocity in the outgoing flow:

$$V_+ = -i \frac{e}{m_i} \left(\frac{\omega_{pi} L}{c} \right)^2 \frac{(2\pi)^{1/2}}{\gamma^{1/2}} \frac{E_*}{\omega} \mathrm{e}^{is^2/2\gamma - i\pi/4}. \tag{III.13}$$

This expression shows that the absolute value of V_+ is independent of s, which means that the particle has already left the resonance. Yet, it has not moved far enough into the low field area to convert its gyro-velocity into parallel velocity. This is consistent with the

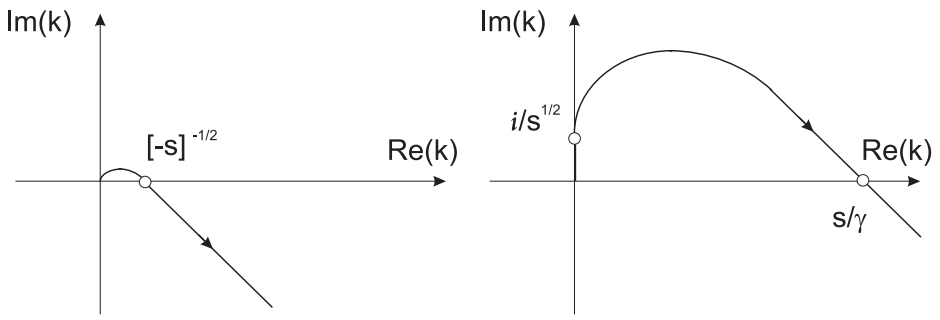

FIG. 2: Saddle points (open circles) and contour C_2 for $s \to -\infty$ (left) and $s \to \infty$ (right). The contours start at the origin and go to $|k| \to \infty$. The arrows on the contours indicate the direction of the integration.

assumption that the width of the resonance is much smaller than the equilibrium magnetic field scale-length L.

The k_3 saddle point represents the evanescent wave field in the outgoing flow:

$$E_+ = -iE_*\sqrt{\pi}s^{1/4}\mathrm{e}^{-2\sqrt{s}}. \tag{III.14}$$

A remarkable feature of the solution described above is the absence of a reflected wave, which means 100% conversion of the incident rf-wave energy into the ion gyro-motion.

A similar asymptotic analysis of the solutions represented by C_1 and C_3 shows that none of them meets the boundary conditions for our problem. The C_1 solution gives a diverging wave field at $s = +\infty$, and the C_3 solution gives a non-zero ion gyro-velocity at $s = -\infty$.

It should be noted that for large values of γ Eqs.(III.12) and (III.13) can be combined into a WKB-type solution for V_+, which is valid not just asymptotically, but for all s:

$$V_+ = -i\frac{e}{m_i}\left(\frac{\omega_{pi}L}{c}\right)^2\sqrt{\frac{2\pi}{|\varphi''(k_*)|}}\frac{E_*}{\omega}\mathrm{e}^{\varphi(k_*)}\mathrm{e}^{-i\pi/4}. \tag{III.15}$$

Here k_* is the positive real root of the cubic equation (III.10). Indeed, for large values of γ the function e^{φ} on the steepest descent line is localized in a close vicinity of the saddle point k_* regardless of s. This can be seen from the Taylor expansion of $\varphi = i(ks - 1/k - \gamma k^2/2)$ around the saddle point:

$$\varphi(k) = i(k_*s - 1/k_* - \gamma k_*^2/2) - i\frac{(k-k_*)^2}{2k_*^2}(\gamma k_*^2 + 2/k_*). \tag{III.16}$$

Eq.(III.16) allows us to estimate the width of the localization interval $|k - k_*|$ as

$$|k - k_*| \sim k_*(\gamma k_*^2 + 2/k_*)^{-1/2} < k_*/\gamma^{1/6} \ll k_*. \tag{III.17}$$

Fig.3 shows that k_* increases continuously from 0 to $+\infty$ as s goes from $-\infty$ to $+\infty$. The existence of the global WKB-type solution (III.15) for large values of γ reflects the fact that the incident wave energy flux transforms into the energy flux of the rotating ions over many wave-lengths.

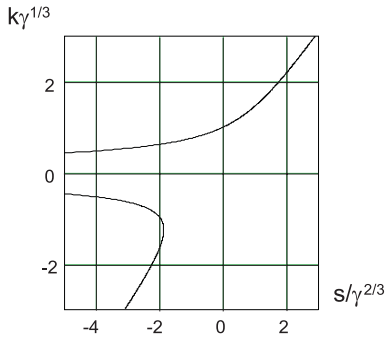

FIG. 3: Real roots of Eq. (III.10). The upper curve shows $k_*(s)$, the relevant root for the WKB solution given by Eq. (III.15).

In order to estimate the spatial width of the transformation interval, δ, we use the condition that the energy flux transformation takes place in the area where the wave group-velocity is comparable to the ion flow velocity. An equivalent requirement is that all three terms on the left hand side of Eq.(III.10) are of the same order of magnitude. This requirement gives

$$\delta = \frac{c^2}{L\omega_{pi}^2}\gamma^{2/3}, \gamma \gg 1. \tag{III.18}$$

In the limiting case of $\gamma \ll 1$ (slow incoming ions), the width of the transformation interval becomes much smaller than the scale-length of the wave electric field near the resonance. The corresponding estimate for δ follows from the condition that the convective term on the left hand side of Eq.(II.18) is comparable to the second term on the right hand side. The result is

$$\delta = \frac{c^2}{L\omega_{pi}^2}\gamma^{1/2}, \gamma \ll 1. \tag{III.19}$$

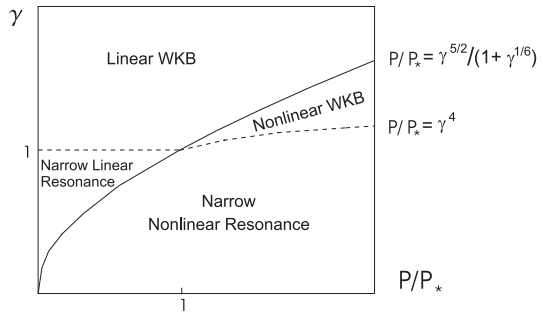

FIG. 4: Map of absorption regimes in the (γ, P) plane. Solid curve marks the border between linear and nonlinear regimes. Dashed curve shows the applicability boundary for WKB-description. The Narrow Nonlinear Resonance area corresponds to significant reflection of the incident wave.

It is convenient to combine Eqs.(III.18) and (III.19) into the following interpolation formula for δ:

$$\delta = \frac{c^2}{L\omega_{pi}^2}\left(\gamma^{2/3} + \gamma^{1/2}\right). \tag{III.20}$$

To conclude this section, we formulate the applicability condition for the linear theory. The constraint comes from the requirement that the relative change of the flow velocity, $\Delta V_z/V_z$, is small within the flux transformation interval. Eq.(II.20) allows us to estimate $\Delta V_z/V_z$ as

$$\frac{\Delta V_z}{V_z} \sim \frac{\delta}{V_z^2}\frac{V_+^2}{L} \sim \frac{\delta}{V_z^3}\frac{P}{m_i n L}, \tag{III.21}$$

where

$$P = \frac{c^2|E_*|^2}{4\omega L}\left[\frac{\omega_{pi}L}{c}\right]^2$$

is the incident power flux. Here we take into account that

$$nV_z\frac{m_i V_+^2}{2} \sim P \tag{III.22}$$

in the transformation area. It is easy to verify that the contribution from the $|B_+|^2$-term on the right hand side of Eq.(II.20) does not affect our estimate for $\Delta V_z/V_z$. The contribution from the c_s^2-term is insignificant as well, since we are only interested in the supersonic flow.

We finally use Eq.(III.20) for δ and the relationship between V_z and γ, Eq.(III.2), to write the condition $\Delta V_z/V_z \ll 1$ in the form

$$P \ll P_* \frac{\gamma^{5/2}}{1+\gamma^{1/6}}, \tag{III.23}$$

where P_* is defined as

$$P_* \equiv m_i n c^3 \left(\frac{L\omega}{c}\right)^3 \left(\frac{c}{L\omega_{pi}}\right)^{10}. \tag{III.24}$$

Eq.(III.23) gives the boundary between the linear and nonlinear regimes in the $(\gamma; P)$ plane. This boundary is shown in Fig.4 by the solid curve with the linear regime above the curve and nonlinear regime below.

IV. NONLINEAR RESONANCE

We will start this section by generalizing the WKB solution to the nonlinear case. The idea behind this generalization is that the WKB approximation remains accurate at the boundary where the linear theory breaks down, provided that $P > P_*$. Therefore, for $P > P_*$, the WKB approach can be extended somewhat below the solid line in Fig.4. We will show that the corresponding area is bounded from below by the condition

$$P \ll P_* \gamma^4 \tag{IV.1}$$

as indicated by the dashed curve in Fig.4.

A Nonlinear WKB Solution

In the WKB-solution, the quantities E_+, B_+, and V_+ are characterized by a fast exponential dependence on z

$$\mathrm{e}^{i\int^z k(\tilde{z})d\tilde{z}}, \tag{IV.2}$$

where k is a local wave number that is real for all z in our solution. We then seek V_+ in the form

$$V_+ = V(z)\mathrm{e}^{i\int^z k(\tilde{z})d\tilde{z}}, \tag{IV.3}$$

where $V(z)$ is a slowly varying amplitude.

We now use Eqs.(II.16) and (II.17) to lowest order to find

$$E_+ = i\frac{4\pi ne\omega}{k^2c^2}V_+, B_+ = -\frac{4\pi ne}{kc}V_+, \tag{IV.4}$$

and we substitute E_+ into Eq.(II.18) to obtain the local dispersion relation

$$kV_z = \frac{\omega\omega_{pi}^2}{k^2c^2} + \omega\frac{z}{L}. \tag{IV.5}$$

Next, we write down the energy balance equation (conservation of the energy flux), an exact consequence of Eqs.(II.16)-(II.19):

$$nV_z\frac{m_i|V|^2}{2} + \frac{ic}{8\pi}\left(E_+B_+^* - E_+^*B_+\right) = P = const. \tag{IV.6}$$

We use this equation together with (IV.4) to find $|V|^2$:

$$|V|^2 = P\frac{4\pi e^2}{m_i^2}\left[\frac{\omega_{pi}^2V_z}{2} + \frac{\omega\omega_{pi}^4}{k^3c^2}\right]^{-1}. \tag{IV.7}$$

When combined with the condition $V_z = const$, Eqs.(IV.3)-(IV.5) and (IV.7) reproduce the WKB solution for the linear problem discussed in Sec.III.

The difference between the nonlinear and the linear WKB-problems is that V_z and n are not constant anymore in the nonlinear case. The condition $V_z = const$ should now be replaced by the longitudinal momentum balance equation, Eq.(II.20), that reduces to

$$\frac{\partial}{\partial z}\left[\omega_{pi}^2V_z^2 + \frac{\omega_{pi}^4}{2k^2c^2}|V|^2\right] = \frac{|V|^2}{2L}. \tag{IV.8}$$

As before, we have neglected the c_s^2-term in this equation, as we assume the flow to be supersonic.

It follows from Eq.(IV.5) that

$$1/L = \frac{\partial}{\partial z}\left[\frac{kV_z}{\omega} - \frac{\omega_{pi}^2}{k^2c^2}\right], \tag{IV.9}$$

which allows us to rewrite Eq.(IV.8) in the form

$$\frac{\partial}{\partial z}\left[\omega_{pi}^2V_z^2 + \frac{\omega_{pi}^4}{2k^2c^2}|V|^2\right] = \frac{|V|^2}{2}\frac{\partial}{\partial z}\left[\frac{kV_z}{\omega} - \frac{\omega_{pi}^2}{k^2c^2}\right]. \tag{IV.10}$$

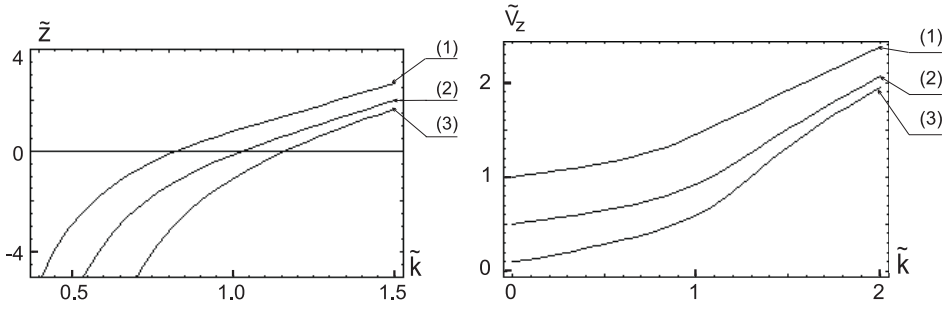

FIG. 5: Solutions of Eqs. (IV.11) and (IV.12) for three different values of $\tilde{V}_z$ at $\tilde{z} \to -\infty$: (1) $\tilde{V}_z(-\infty) = 1$; (2) $\tilde{V}_z(-\infty) = 0.5$; (3) $\tilde{V}_z(-\infty) = 0.1$.

A rescaling transformation from k, V_z, and z to new (dimensionless) variables $\tilde{k}$, $\tilde{V}_z$, and $\tilde{z}$ allows us to rewrite Eqs.(IV.5) and (IV.10) as follows:

$$\tilde{z} = \frac{\tilde{k}^3\tilde{V}_z^2 - 1}{\tilde{k}^2\tilde{V}_z}, \tag{IV.11}$$

$$\frac{d\tilde{V}_z}{d\tilde{k}} = \tilde{V}_z \frac{\tilde{k}^6\tilde{V}_z^4 + 6\tilde{k}^3\tilde{V}_z^2 + 2}{2\tilde{V}_z(\tilde{k}^3\tilde{V}_z^2 + 2)^2 - \tilde{k}(\tilde{k}^6\tilde{V}_z^4 + 5\tilde{k}^3\tilde{V}_z^2 + 2)}. \tag{IV.12}$$

Here

$$\tilde{k} = \frac{ck}{\omega}\left[\frac{m_i c\omega^2}{\pi e^2 j}\right]^{3/5}\left[\frac{\pi e^2 P}{m_i^2 c^3\omega^2}\right]^{2/5}, \tag{IV.13}$$

$$\tilde{V}_z = \frac{V_z}{2c}\left[\frac{\pi e^2 j}{m_i c\omega^2}\right]^{2/5}\left[\frac{m_i^2 c^3\omega^2}{\pi e^2 P}\right]^{3/5}, \tag{IV.14}$$

$$\tilde{z} = \frac{z}{2L}\left[\frac{m_i c\omega^2}{\pi e^2 j}\right]^{1/5}\left[\frac{m_i^2 c^3\omega^2}{\pi e^2 P}\right]^{1/5}. \tag{IV.15}$$

The applicability condition for the WKB solution is

$$\frac{1}{k^2}\frac{dk}{dz} \ll 1. \tag{IV.16}$$

In dimensionless variables, we have

$$\frac{c}{2\omega L}\left[\frac{\pi e^2 P}{m_i^2 c^3\omega^2}\right]^{1/5}\left[\frac{m_i c\omega^2}{\pi e^2 j}\right]^{4/5}\frac{1}{\tilde{k}^2}\frac{d\tilde{k}}{d\tilde{z}} \ll 1. \tag{IV.17}$$

Since $\tilde{k}$ and $d\tilde{k}/d\tilde{z}$ are quantities of order unity at the transformation point, this constraint reduces to

$$\frac{c}{2\omega L}\left[\frac{\pi e^2 P}{m_i^2 c^3 \omega^2}\right]^{1/5}\left[\frac{m_i c\omega^2}{\pi e^2 j}\right]^{4/5} \ll 1, \tag{IV.18}$$

which is equivalent to Eq.(IV.1).

Numerical solutions of Eqs.(IV.11) and (IV.12) for three different values of initial flow velocity are shown in Fig.5. We find that $\tilde{V}_z$ and $\tilde{k}$ are monotonically increasing functions of $\tilde{z}$. Their asymptotic behavior for $\tilde{z} \to +\infty$ is given by

$$\tilde{k} = \tilde{V}_z = \sqrt{\tilde{z}}. \tag{IV.19}$$

B Narrow Nonlinear Resonance

In this subsection, we will consider the non-linear regime lying below the dashed curve in Fig.4. We have shown that the dashed curve is where the WKB-approximation breaks down. One can thus conjecture that the width of the energy transformation layer should be smaller than the scale-length of the wave electric field if P and γ are below the dashed curve. In fact, we have already shown that the resonance is indeed narrow in the linear regime for $\gamma \ll 1$. We now extend the narrow-resonance approach to the nonlinear case. In other words, we make a verifiable assumption that the wave electric field is independent of z in the energy transformation layer. It can also be verified that the $|B_+|^2$-term, as well as the c_s^2-term, in Eq.(II.20) is negligibly small in the narrow-resonance case. As a result, Eqs.(II.18) and (II.20) can be simplified to:

$$V_z \frac{\partial V_+}{\partial z} = \frac{e}{m_i} E_0 + i\omega \frac{z}{L} V_+, \tag{IV.20}$$

$$V_z \frac{\partial V_z}{\partial z} = \frac{|V_+|^2}{2L}, \tag{IV.21}$$

where E_0 is the value of E_+ at $z = 0$. We solve Eqs.(IV.20) and (IV.21) with the boundary conditions:

$$V_+(z = -a) = i\frac{eL}{m_i a} E_0, V_z(z = -a) = u, \tag{IV.22}$$

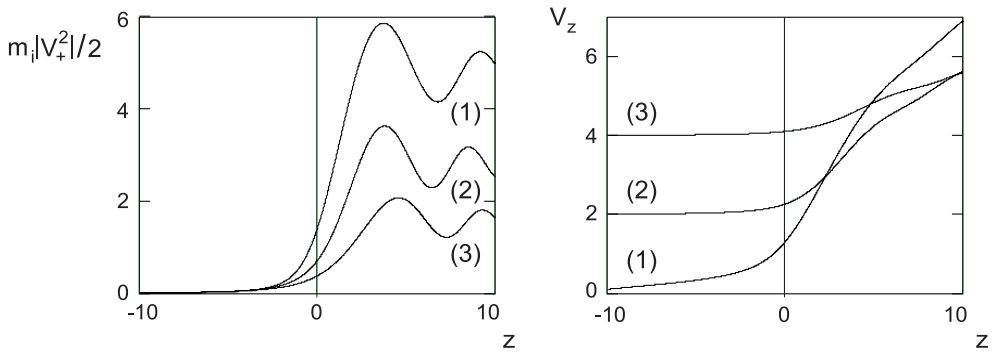

FIG. 6: Solutions of Eqs. (IV.20), (IV.21) for three different values of the incident flow velocity u: (1) $u = 0.1$; (2) $u = 2$; (3) $u = 4$. The flow velocity V_z is normalized to $L\omega \left[\frac{eE_0}{m_i L\omega^2}\right]^{4/5}$. The rotational energy $m_i|V_+|^2/2$ and distance from the resonance z are normalized to $\frac{m_i}{2}L^2\omega^2 \left[\frac{eE_0}{m_i L\omega^2}\right]^{6/5}$ and $L\left[\frac{eE_0}{m_i L\omega^2}\right]^{2/5}$ respectively.

where u is the incident flow velocity and a is an outer boundary for the narrow layer solution. It should be noted that u is generally different from V_0 because the flow may accelerate between $z = -\infty$ and $z = -a$, i.e. before the ions enter the narrow transformation layer. The value of a needs to be chosen to satisfy the condition:

$$\delta \ll a \ll \delta_E, \tag{IV.23}$$

where δ_E is the scale-length of the wave electric field and δ is the width of the transformation layer. This condition ensures that the physical results are insensitive to a.

Plots of $m_i|V_+|^2(z)/2$ and $V_z(z)$ for different values of u are shown in Fig.6. Note that the change in V_z is relatively small for large values of u, which corresponds to the linear regime discussed in Sec.III. The change in V_z becomes more significant as u decreases, so that the problem becomes essentially nonlinear. An important feature of the nonlinear regime is that the ion energy gain tends to a finite limit as u goes to zero. This means that the nonlinearity limits the particle energy gain. In the limit of small u this energy gain per particle is roughly $jL^2\omega^2 \left[\frac{e|E_0|}{m_i L\omega^2}\right]^{6/5}$ as opposed to $jL^2\omega^2 \frac{L\omega}{V_z}\left[\frac{e|E_0|}{m_i L\omega^2}\right]^2$ in the linear regime. This shows that for a given particle flux, the total energy flux in the outgoing flow is independent of the flow velocity in the linear regime, and that the outgoing energy flux decreases as the particle motion becomes nonlinear. As the particles are now unable to carry away all of the incident

wave energy, a significant part of the energy must go into a reflected wave. Another way to understand the reflection is to take into account that the ion density exhibits a steep drop in the nonlinear regime, which happens over a distance that is shorter than the wave-length. This can roughly be viewed as a discontinuity in a dielectric constant which usually causes partial reflection.

In order to find the reflection coefficient one would need to match the narrow resonance solution, described in this section, to the outer solution of Eqs.(II.16)-(II.20). This matching is straightforward when the linear approximation applies to the outer solution, so that the ion density does not change considerably over the interval from $z = -\infty$ to $z = -\delta_E$. Our estimates show that this requires $P/P_* < \gamma^2$. However, if P is greater than $P_*\gamma^2$, the outer solution itself is essentially nonlinear, which complicates the matching problem. One might think of using a WKB approximation to find the nonlinear outer solution, but the presence of a reflected wave will most likely preclude such an approach. The reason is that the interference between the incident and reflected waves will cause modulations of $|V_+|^2$, V_z, and n on a wave-length scale. This modulation can easily enhance the reflection or may even become the primary reflection mechanism. Because of its technical difficulty we will address the nonlinear reflection problem numerically rather than analytically. The corresponding calculations are described in the next section.

V. GLOBAL PICTURE

The set of Eqs.(II.16)-(II.20) derived in Sec.II is limited to a narrow region near the ion cyclotron resonance. In order to describe a broader spatial interval, we need to take into account:

a) the electron current,

b) deviation from the linear profile of the equilibrium magnetic field.

In the ion-cyclotron frequency range, the $\mathbf{E}\times\mathbf{B}$ drift gives rise to $x-$ and $y-$components of the electron current,

$$j^e_\alpha = -e_{\alpha\beta\gamma}E_\beta \frac{B_{0\gamma}}{|B_0|}\frac{\omega^2_{pe}}{4\pi|\omega_{ce}|}, \tag{V.1}$$

where where $e_{\alpha\beta\gamma}$ is the completely antisymmetric unit tensor. This electron current is comparable to the ion current away from the resonance, which is why it becomes important in the global picture.

Generalization from the near-resonance expression, Eq.(II.1), to an arbitrary profile $B_{0z}(z)$ involves generalization of the quantities E_+, B_+, and V_+. In this section, we define E_+ as

$$E_+ \equiv \frac{E_x + iE_y}{\sqrt{B_{0z}/B_*}}, \tag{V.2}$$

where B_* is the value of the magnetic field at the point $\omega = \omega_{ci}$. The new expressions for B_+ and V_+ are similar to Eq.(V.2). It should be noted that these generalized definitions of E_+, B_+, and V_+ are fully consistent with the ones we used in the local description.

We will skip a straightforward derivation of the generalized set of equations and just present the modified equations in their final form:

$$\frac{\partial E_+}{\partial z} = \frac{\omega B_+}{c}, \tag{V.3}$$

$$\frac{\partial B_+}{\partial z} = \frac{\omega_{pi}^2}{\omega_{ci} c} E_+ - \frac{4\pi i}{c} n e V_+, \tag{V.4}$$

$$V_z \frac{\partial V_+}{\partial z} = \frac{e}{m_i} E_+ + i(\omega - \omega_{ci}) V_+, \tag{V.5}$$

$$V_z \frac{\partial V_z}{\partial z} = -\frac{1}{8\pi m_i n} \frac{B_{0z}}{B_*} \frac{\partial |B_+|^2}{\partial z} - \frac{|V_+|^2}{2B_*} \frac{\partial B_{0z}}{\partial z} - \frac{c_s^2}{n} \frac{\partial n}{\partial z}, \tag{V.6}$$

$$\frac{B_*}{B_{0z}} n V_z \equiv j = const. \tag{V.7}$$

This set of equations now describes both the resonant conversion of the incident wave energy into the ion rotational energy and the subsequent transformation of the ion rotation into their fast motion along the decreasing magnetic field.

We solve Eqs.(V.3)-(V.7) numerically for $s = 0$ and for a specific profile of the equilibrium magnetic field:

$$B_{0z} = B_* \left[1 - \frac{z}{\sqrt{L^2 + z^2}} \right]. \tag{V.8}$$

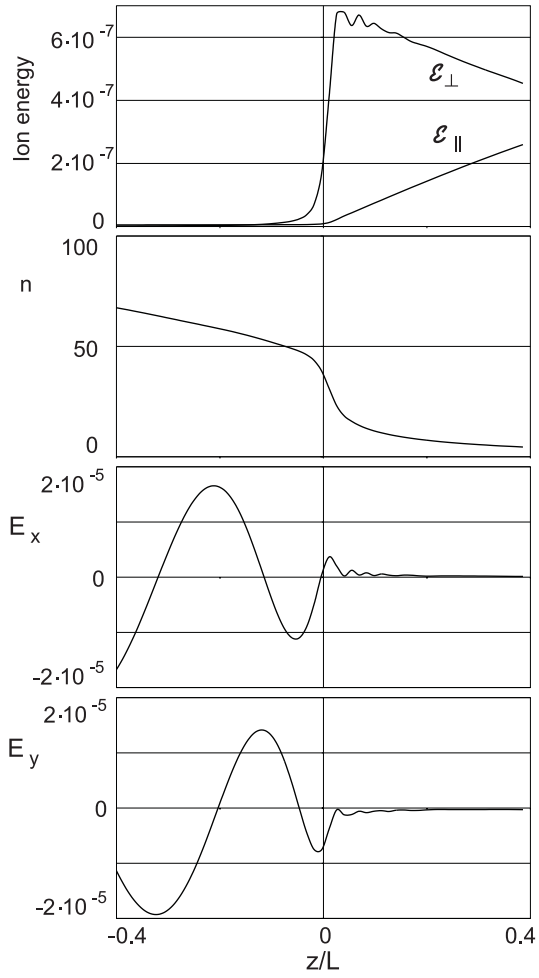

FIG. 7: Solution of Eqs. (V.3)-(V.7) for $j = 5 \cdot 10^5 (m_i \omega c^2)/(4\pi L e^2)$, $\bar{n} = 100 \cdot m_i c^2/4\pi e^2 L^2$, and $|\bar{E}| = \sqrt{10} \cdot 10^{-5} \cdot m_i L \omega^2/e$. The quantities $\mathcal{E}_\perp \equiv m_i |V_+|^2 B_{0z}/2B_*$ and $\mathcal{E}_{||} \equiv m_i V_z^2/2$ are normalized to $m_i L^2 \omega^2$. The ion density n and the electric field components E_x and E_y are normalized to $m_i c^2/4\pi e^2 L^2$ and $m_i L \omega^2/e$ respectively.

This expression represents the near-axis field of an open-ended solenoid. Our code integrates Eqs.(V.3)-(V.7) starting from the strong field side with an adjustable boundary condition at a large negative value of z. The code employs a shooting procedure to find the solution for which E_+ and B_+ vanish in the outgoing flow (at $z \to \infty$). This allows us to automatically determine the amplitude of the reflected wave in the case of nonlinear reflection. Each solution is characterized by three parameters: the particle flux j, the mean density $\bar{n}$ and the mean electric field amplitude $|\bar{E}|$ in the incident flow ($z \to -\infty$).

Figs.7 and 8 show a solution that represents a moderately nonlinear regime. The density

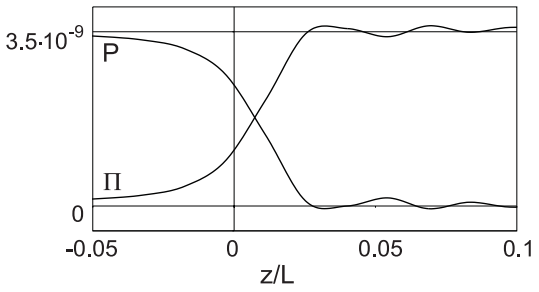

FIG. 8: Conversion of the Poynting vector P into the ion power flux Π. The plot corresponds to the solution presented in Fig. 7. The quantities P and Π are normalized to $Lm_i^2c^2\omega^3/4\pi e^2$.

plot in Fig.7 already exhibits a steep gradient near the resonance but with a very minor reflection yet. The amount of reflection can be inferred from the oscillations of $|E|^2 \equiv E_x^2+E_y^2$ shown in Fig.9. These oscillations represent an interference between the incident and the reflected waves. The oscillations become more pronounced in the case of a stronger rf-field or slower ion flow. Related to the reflection are density and velocity modulations in the incoming flow. As seen from Fig.9(right), the decrease in the flow velocity can produce a larger reflection even when the rf-field is weaker that that shown in Fig.9(left).

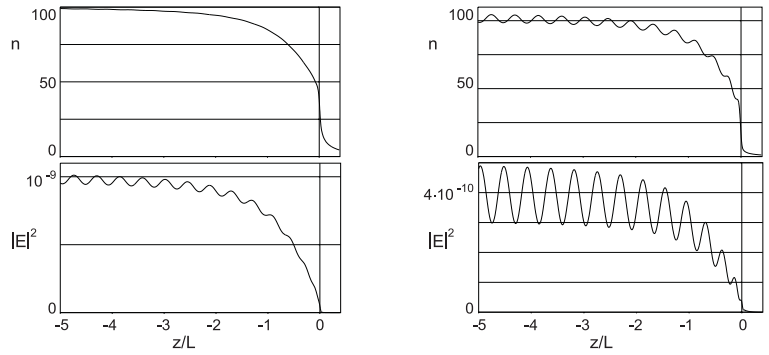

FIG. 9: Modulation of the wave amplitude and ion density due to nonlinear reflection from the resonance. Left plots correspond to the solution presented in Fig. 7. Right plots correspond to the solution with $j = 1.5 \cdot 10^5(m_i\omega c^2)/(4\pi Le^2)$, $\bar{n} = 100 \cdot m_ic^2/4\pi e^2L^2$, and $|\bar{E}| = 2 \cdot 10^{-5} \cdot m_iL\omega^2/e$. Quantities n and $|E|^2$ are normalized to $m_iL^2\omega^2$ and $m_i^2L^2\omega^4/e^2$ respectively.

VI. SUMMARY

We have presented a self-consistent nonlinear model for the deposition of rf-power in the ion cyclotron frequency range into a steady state plasma flow. This work can be viewed as a nonlinear version of the magnetic beach problem [4] for ion-cyclotron waves. We find that the absorption coefficient for the wave is 100% as long as either linear theory or WKB approximation applies to the problem. Acceleration of the incoming ions due to the energy deposition from the wave adds nonlinear features to the absorption process. The longitudinal forces create a density gradient in the ion flow, which causes partial reflection of the incident rf-power. The reflection is most pronounced when the characteristic scale-length of the density drop becomes shorter than the wavelength. An interesting consequence of this nonlinear reflection is the spatial modulation of the incident flow. Simple one-dimensional fluid-type simulations, described in this paper, confirm our theoretical picture of the near-resonance behavior and allow us to quantitatively model the entire process of wave energy conversion into the directed energy of the ion flow. We envisage two natural extensions of the presented work. First, our single-fluid model can be generalized to the case of several groups of ions with different parallel velocities. This should allow us to evaluate the role of the ion velocity spread in the incident flow. Second, for practical applications like VASIMR, the basic nonlinear effects discussed in this paper need to be combined with two-dimensional calculations of the wave field. The need for such an extension becomes evident if one takes into account that the finite plasma radius should definitely affect the field structure in a realistic geometry.

ACKNOWLEDGMENTS

This work was supported by the VASIMR Plasma Thruster project at NASA and by the U.S.Department of Energy Contract No. DE-FG03-96ER-54346. We thank Dr. Franklin Chang-Diaz, Dr. Roger Bengtson, and Dr. Andrew Ilin for stimulating discussions.

REFERENCES

[1] F.R.Chang Diaz, M.M.Hsu, T.F.Yang, "Rapid Mars Transit With Exhaust-Modulated Plasma Proplsion", *NASA Technical Paper*, 3539 (1995).

[2] F.R.Chang Diaz, et.al.,"The Development of VASIMR Engine", Proc. Int. Conf. on Electromagnetics in Advanced Applications (ICEAA'99), Torino, Italy.

[3] M.Martinez-Sanchez, J.E.Pollard, "Spacecraft Electric Propulsion - An Overview", *Journal of Propulsion and Power*, **14**, 688-699 (1998).

[4] T.H.Stix, "Waves in Plasmas" p.342 (AIP New York 1992),

[5] T.H.Stix, "Waves in Plasmas" p.354 (AIP New York 1992).